The effect of spin orbit interaction on the physical properties of $LaTSi_3$ (T = Ir, Pd, and Rh): First-principles calculations

H. Y. Uzunok, H. M. Tütüncü, G. P. Srivastava, E. İpsara, and A. Başoğlu

Citation: Journal of Applied Physics **121**, 193904 (2017); doi: 10.1063/1.4983770

View online: http://dx.doi.org/10.1063/1.4983770

View Table of Contents: http://aip.scitation.org/toc/jap/121/19

Published by the American Institute of Physics

The effect of spin orbit interaction on the physical properties of $LaTSi_3$ (T = Ir, Pd, and Rh): First-principles calculations

H. Y. Uzunok,[1,2] H. M. Tütüncü,[1,2] G. P. Srivastava,[3] E. İpsara,[1] and A. Başoğlu[1,2]
[1]*Sakarya Üniversitesi, Fen-Edebiyat Fakültesi, Fizik Bölümü, 54187 Sakarya, Turkey*
[2]*Sakarya Üniversitesi, Biyomedikal, Manyetik ve Yarıiletken Malzemeler Araştırma Merkezi (BIMAYAM), 54187 Sakarya, Turkey*
[3]*School of Physics, University of Exeter, Stocker Road, Exeter EX4 4QL, United Kingdom*

(Received 14 February 2017; accepted 8 May 2017; published online 19 May 2017)

We have presented the structural, elastic, electronic, phononic, and electron-phonon interaction properties of the La-based noncentrosymmetric superconductors, such as $LaIrSi_3$, $LaRhSi_3$, and $LaPdSi_3$, by using the generalized gradient approximation of the density functional theory. The calculated elastic constants reveal the mechanical stability of all the studied compounds in their noncentrosymmetric structure, while the lack of inversion symmetry gives rise to lift the degeneracy of their electronic bands, except in the Γ-Z and X-P directions. The calculated Eliashberg spectral function shows that all phonon branches of these materials couple considerably with electrons, and thus, all of them make contribution to the average electron-phonon coupling parameter λ. Using the calculated values of λ and the logarithmically averaged phonon frequency ω_{ln}, the superconducting critical temperature T_c values for $LaIrSi_3$, $LaRhSi_3$, and $LaPdSi_3$ are estimated to be 0.89, 2.56, and 2.40 K, respectively, which accord very well with their corresponding experimental values of 0.77, 2.16, and 2.60 K. *Published by AIP Publishing.* [http://dx.doi.org/10.1063/1.4983770]

I. INTRODUCTION

In recent years, $BaNiSn_3$-type $LnTX_3$ compounds (Ln: a lanthanide element; T: a transition metal; and X: Si and Ge) have been widely investigated because of their interesting physical properties such as valence fluctuations[1–3] and different magnetic properties.[4–9] Furthermore, $CeRhSi_3$,[10,11] $CeIrSi_3$,[12–14] $CeCoGe_3$,[15,16] and $CeIrGe_3$ (Ref. 17) with $BaNiSn_3$-type structure have been found to exhibit pressure-induced superconductivity. This finding is very interesting because their structure lacks inversion symmetry along the c-axis. Thus, the absence of inversion symmetry of a crystal introduces a Rashba-type antisymmetric spin orbit coupling (ASOC) that can cause some unconventional character of superconductivity, i.e., revealing a mixture of spin-singlet and spin-triplet pairings.[18,19] However, these Ce-based noncentrosymmetric superconductors (NCS) are placed close to a magnetic quantum critical point, making it difficult to discover the effects of ASOC and inversion symmetry breaking on superconductivity. In order to explore the influence of inversion symmetry breaking on superconductivity, nonmagnetic Rashba-type NCS must be discovered and studied because the extra complications that originate from strong f-electron correlations can be prohibited. Thus, several f-electron-free NCS have also been reported such as $BaPtSi_3$,[20,21] $LaRhSi_3$,[22,23] $CaPtSi_3$,[24,25] $CaIrSi_3$,[24,25] $LaPtSi_3$,[26] $LaPdSi_3$,[26] $LaIrSi_3$,[27] and $SrAuSi_3$.[28] These $BaNiSn_3$-type NCS do not show strong electronic correlations, and moreover, superconductivity takes place at ambient pressure with conventional BCS character. The electronic properties of these $BaNiSn_3$-type NCS can affect their superconducting properties due to electron-phonon interactions. Due to this reality, Terashima *et al.*[29] have reported the de Haas-van Alphen (dHvA) effect at ambient pressure and band-structure calculations for $LaRhSi_3$ and $CeRhSi_3$. This experimental study indicated that frequency branches in $CeRhSi_3$ differ from the ones in $LaRhSi_3$. This result proposes that the Fermi surface mapping in $CeRhSi_3$ differs from that in $LaRhSi_3$, which can be linked to the contribution of the Ce 4f electrons. Furthermore, from the results of the dHvA measurement for $LaIrSi_3$ (Ref. 30), it is found that the Fermi surface is split into two surfaces due to the spin-orbit interaction (SOI).

On the theoretical side, the full-potential-linearised augmented plane wave (FLAPW) method has been utilized to investigate the electronic band structures and Fermi surfaces of $LaIrSi_3$ (Ref. 30) and $LaRhSi_3$.[29] Both the previous theoretical works[29,30] indicated that all atoms contribute to energy bands near the Fermi level. Following these theoretical works, the electronic and lattice dynamical properties of $BaPtSi_3$ (Ref. 20) have been studied by using the density functional theory within the local density approximation (LDA). This theoretical work indicated that the spin-orbit splitting of the relativistic electronic bands is very small at the Fermi level, and thus, superconductivity keeps to an almost undisturbed BCS state. The FLAPW method has been employed to investigate the structural and electronic properties of $CaIrSi_3$ and $CaPtSi_3$.[31] This theoretical work indicated that the near Fermi valence bands in both materials derive from transitional metal's d orbitals with an admixture of Si p orbitals. Furthermore, relativistic LDA calculations have been made for obtaining electronic properties of these NCS.[32] The calculated electronic structure of both materials shows similarities to that of the other NCS $BaPtSi_3$.[20] The electronic properties of $LaPdSi_3$ have been studied employing the full-potential local-orbital method within density functional theory.[33] This theoretical work mentioned that the strength of an antisymmetric spin orbit coupling in this

material is comparable to that of $BaPtSi_3$. The FLAPW method has been used to investigate the electronic properties of $SrAuSi_3$.[28] This theoretical work concluded that the spin-orbit interaction for this NCS has only little influence on the band structure around the Fermi level. Furthermore, this theoretical work suggests that the mechanism of superconductivity in this material is phonon mediated. These theoretical works are not complete enough to explain the origin of superconductivity in these NCS because their phonon properties must be calculated to study electron-phonon interaction. This reality motivated Arslan *et al.*[34] to study the electron-phonon interaction in $SrAuSi_3$. This work has been done with and without spin-orbit interactions. This theoretical work stated that the influence of spin-orbit coupling on the phonon frequencies and their electron-phonon coupling parameter is very small. Thus, this theoretical work supported that this material is phonon mediated superconductor with weak electron-phonon coupling. Furthermore, Uzunok *et al.*[35] have employed an *ab initio* study of electronic, vibrational, and electron-phonon interaction properties of body-centred tetragonal $CaIrSi_3$ by employing the density functional theory, a linear response formalism, and the plane-wave pseudopotential method. They concluded that the effect of spin-orbit interaction on the electron-phonon interaction properties of this material is rather small, which can be related to the negligible influence of this interaction on the band structure around the Fermi level.[35]

In this paper, we examine the origin of superconductivity in La-based NCS, such as $LaIrSi_3$, $LaRhSi_3$, and $LaPdSi_3$, because no magnetic order is available for these materials to interfere with their superconducting state. In addition to this, these materials do not show strong electronic correlations and exhibit superconductivity with the BCS characteristics at ambient pressure. In contrast, a majority of Ce-based NCS[12–17] are antiferromagnetic and become superconducting only under pressure. Hence, La-based NCS are good choice to research for the effect of spin-orbit interaction on their physical properties.

Although sufficient theoretical works have been made on the electronic properties of $LaTSi_3$, no theoretical works exist for their vibrational and electron-phonon interaction properties. However, the electron-phonon interaction determines a number of important physical properties of metals such as electrical and thermal resistivities, thermal expansion, and superconductivity. Keeping in mind the significant role of electron-phonon interaction in the establishment of BCS-type superconductivity, in this study, we have made *ab initio* planewave pseudopotential calculations to obtain the structural, elastic, electronic, phonon properties, and the electron-phonon interaction in the ternary silicides $LaTSi_3$ (T=Ir, Rh, and Pd). The effect of spin orbit interaction on the states close to the Fermi energy for all the considered NCS is presented and discussed in detail. The calculated lattice dynamical properties of all the studied NCS are presented and compared between each other in detail. Moreover, the Eliashberg spectral function[36–38] for all the studied materials has been obtained using the calculated phonon density of states (DOS) and electron-phonon matrix elements. The electron-phonon coupling parameter λ and the logarithmic average of phonon frequency ω_{ln} have been determined from the integration of the Eliashberg spectral function. Inserting these values into the Allen–Dynes formula, the superconducting transition temperatures of all the considered materials are calculated and compared with their experimental values. Finally, an explanation for the difference in their superconducting transition temperatures has been put forward.

II. THEORY

All calculations have been carried out using the density functional theory with and without SOI as implemented in the electronic structure package named Quantum-Espresso.[39] The atomic pseudopotentials formed using the projected-augmented wave[39] (PAW) are used to simulate interactions between valence electrons and ion cores, and the electron wave function is expanded in plane waves up to an energy cutoff of 60 Ry for all calculations. The electronic many-body interaction is explained within the generalized gradient approximation (GGA) of Perdew, Burke, and Ernzerhof (PBE).[40] The Kohn-Sham equations[41] are solved using an iterative conjugate gradient scheme, employing a set of Monkhorst–Pack special $\boldsymbol{k}$ points.[42] The $(8 \times 8 \times 8)$ grid is taken in order to determine the structural parameters, and the electronic structure and electronic density of states are obtained by employing the $(24 \times 24 \times 24)$ grid.

After obtaining self-consistent solutions of the Kohn-Sham equations, the lattice dynamical properties (the phonon spectrum, the density of states, and the eigenvectors corresponding to phonon frequencies) are evaluated within the framework of the self-consistent density functional perturbation theory.[39] For the phonon calculations, Brillouin zone integration has been made by using a set of 59 special **k** points. We have calculated 13 dynamical matrices for a $4 \times 4 \times 4$ **q**-point mesh within the irreducible part of the Brillouin zone. The dynamical matrices at arbitrary wave vectors are then evaluated with the help of a Fourier deconvolution scheme. Finally, the phonon density of states calculations have been performed by using the tetrahedron method. The technique for the calculation of the electron-phonon coupling has been explained in detail in our previous work.[43] The Fermi surface sampling for the evaluation of the electron-phonon matrix elements has been performed using a $(24 \times 24 \times 24)$ $\boldsymbol{k}$-mesh with a Gaussian width of 0.02 Ry.

In order to investigate the mechanical properties of all the studied materials, we have calculated their second-order elastic constants using the method discussed in detail in the theoretical work of Mehl *et al.*.[44] The calculations of the elastic constants need a very high degree of precision because the energy differences involved are of the order less than 1 mRy. To ensure, this requires the use of a fine **k**-point mesh. With our choice of a $(16 \times 16 \times 16)$ **k**-points grid, the energy per atom is converged to 1 mRy or better in all cases. In this study, we have calculated a set of 21 values of $\frac{E(\delta)-E(0)}{V_o} - \delta$ by varying δ from –0.02 to 0.02 in steps of 0.002. Then, these results are fitted to a parabola, and the elastic constants are determined from the quadratic coefficients.

TABLE I. Structural parameters for $LaTSi_3$ and their comparison with the available experimental results.

Material	a(Å)	c(Å)	V(Å^3)	z_T	z_{Si1}	z_{Si2}
$LaIrSi_3$	4.302	9.882	91.43	0.6542	0.4109	0.2625
Experimental[27]	4.278	9.831	89.98	0.6554	0.4110	0.2624
$LaRhSi_3$	4.310	9.878	91.75	0.6559	0.4137	0.2643
Experimental[29]	4.269	9.829	89.58	0.6577	0.4135	0.2650
$LaPdSi_3$	4.375	9.677	92.61	0.6445	0.3915	0.2596
Experimental[26]	4.354	9.664	91.61			

III. STRUCTURAL AND ELECTRONIC PROPERTIES

All the three NCS investigated here belong to $BaNiSn_3$-type tetragonal crystal structure with the space group I4/mm. Each primitive unit cell contains one La atom at the (2a) (0.00, 0.00, 0.00) position, one T atom at 2(a) (0.00, 0.00, z_T), one Si1 atom at 2(a)(0.00, 0.00, z_{Si1}), and two Si2 atoms at the (4b) (0.00, 0.50, z_{Si2}) sites. Thus, two lattice parameters (a and c) and three internal parameters (z_T, z_{Si1}, and z_{Si2}) characterize the crystal structure of all these compounds.

Table I presents the calculated lattice parameters, volume, and internal parameters for all the investigated NCS. Our calculated values for the lattice parameters and internal parameters compare very well with their corresponding experimental values.[26,27,29] In particular, the calculated lattice parameters for all the considered materials differ from their experimental values[26,27,29] within less than 1%, while the maximum difference found for the internal parameters is not more than 0.5%.

As displayed in Fig. 1, each T atom coordinates with one apical Si1 atom and four basal Si2 atoms. Furthermore, each T atom generates a square plane with other three T atoms. In particular, the nearest-neighbor distance Ir-Si1 and Ir-Si2 are calculated to be 2.392 Å and 2.403 Å, which is close to 2.483 Å obtained as the sum of their covalent radii: 1.37 Å for Ir and 1.11 Å for Si. A similar observation has been made for $LaRhSi_3$ and $LaPdSi_3$. These observations indicate that there is a strong covalent bond between T and Si atoms in $LaTSi_3$ compounds. The closest Ir-Ir distance is found to be 4.302 Å, which is much longer the corresponding distance of 2.72 Å in Ir fcc metal. This result proposes the existence of weaker metal-metal interaction in $LaIrSi_3$ as compared with that in the fcc metal Ir. The same situation has been found for the remaining NCS. The values of the Si1-Si2 bond length are calculated to be 2.610, 2.598, and 2.533 Å for $LaIrSi_3$, $LaRhSi_3$, and $LaPdSi_3$, respectively. All these values are larger than the corresponding bond length value of 2.352 Å in diamond Si. This result shows that the covalent Si-Si interaction in all the studied materials is weaker than the corresponding interaction in diamond Si. Some ionic character in these NCS exists due to the difference in the electronegativity among the comprising elements. As a consequence, the bonding in these NCS can be classified as an interplay between covalent, metallic, and ionic characters.

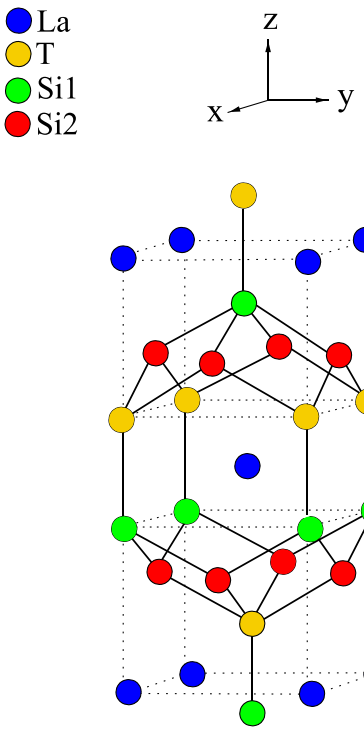

FIG. 1. The $BaNiSn_3$-type crystal structure of $LaTSi_3$. The crystal structure has no mirror plane perpendicular to the z-axis.

Figure 2(a) presents the calculated electronic band structure of $LaIrSi_3$ without and with SOI along various symmetry directions in the Brillouin zone of body-centred tetragonal lattice. Our choice for this compound is that the strength of SOI depends on Z^2 (Z is the atomic number), and thus, we expect that SOI will make more influence on the electronic structure of $LaIrSi_3$ than that of $LaRhSi_3$ (or $LaPdSi_3$) due to the heavier mass of Ir atom than that of Rh atom (or Pd atom). As can be seen from Fig. 2(a), the band structure of $LaIrSi_3$ has a metallic character with at least one band characterized with large dispersion cross the Fermi level along all the considered symmetry directions except along the X-P symmetry direction. Along this symmetry direction, valence and conduction bands are well separated from each other. When SOI is taken into account, the value of splitting between the first pair just above the Fermi level at the Γ point is found to 0.3 eV. The electric field gradient due to the lack of inversion symmetry is also responsible for removing the degeneracy of the electronic bands. However, the two-fold degeneracy of the electronic bands along the Z-Γ and X-P directions still exists, since the ASOC effects only split bands along directions perpendicular to the c-axis. The largest vertical splitting for $LaIrSi_3$ is found along the G1-Z direction just above the Fermi level with the value of 0.35 eV. The electronic band structures of remaining NCS

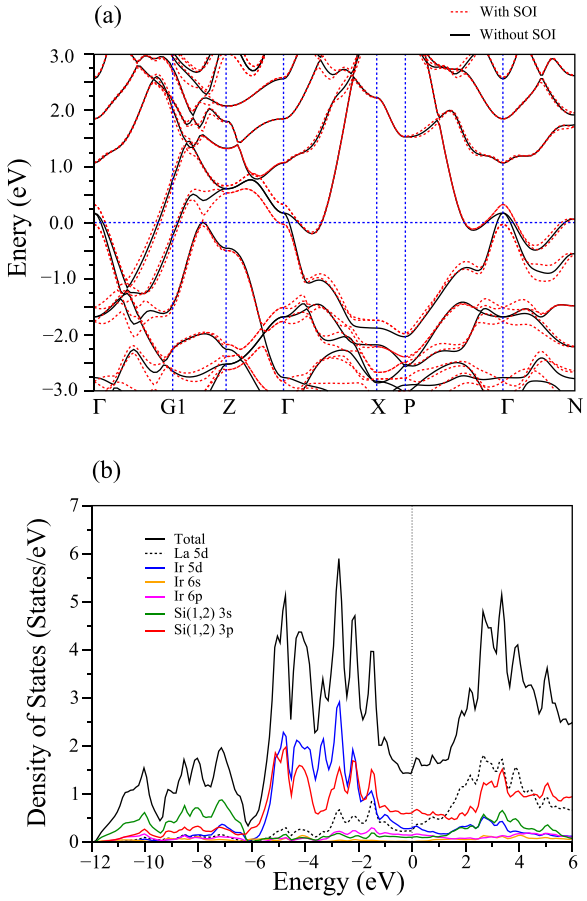

FIG. 2. (a) The calculated electronic band structures of $LaIrSi_3$ along the high symmetry lines in Brillouin zone of body-centred tetragonal lattice with and without SOI. The inclusion of SOI has split several bands. (b) The total and partial electronic density of states with SOI for $LaIrSi_3$.

are rather similar but the band splitting in these materials is much weaker than the corresponding effect in $LaIrSi_3$ because of the smaller mass of Rh atom (or Pd atom) in comparison to that of Ir atom. From these observations, we can conclude that the spin-singlet Cooper pairs dominate in these NCS due to the small splitting of electronic bands close to Fermi level.

In order to identify the nature of electronic bands in the electronic structure of $LaIrSi_3$, we have calculated and presented their total and partial DOS for this material with SOI in Fig. 2(b). We have to mention that the total and partial DOS of other two compounds are also similar to those obtained for $LaIrSi_3$. Now, we will discuss our DOS results for $LaIrSi_3$. Partial DOS of Ir and Si are considerably scattered in the energy window below and above the Fermi level. In particular, for energy window from –6.0 to –3.0 eV, DOS features originate mainly from the 5d states of Ir. However, the contribution of La is very small to the valence band except close to Fermi level. This result is expected because La atoms (with relatively low electronegativity) constitute cations and transfer valence electrons to $IrSi_5$. Thus, the interaction between La and $IrSi_5$ is rather ionic. The intensity patterns of the partial DOS of the Ir and Si states look similar over the wide energy range around the Fermi level. This result shows that the Ir d and Si p states strongly hybridize and form covalent bond between them. Examination of the valence DOS features for $LaIrSi_3$ confirms that the bonding situation in this material is a mixture of covalent and ionic bonds. Although the contributions of the Si(1,2) atoms dominate near the Fermi level, all three atomic species contribute to the bands at and just above the Fermi level. This result indicates that La in this material is not totally ionized to the 3^+ state. The value of the DOS at the Fermi level $N(E_F)$ is estimated to be 1.47 states/eV with SOI, which is slightly smaller than the value of 1.57 states/eV without SOI. This result re-confirms that the effect of SOI on the bands close to Fermi level is very small. The contributions of La, Ir, and Si(1,2) to $N(E_F)$ are approximately 18%, 32%, and 50%, respectively. In particular, the orbital characters at the Fermi level are mainly composed of Si2 3p (23%), Ir 5d(21%), Si1 3p(20%), La 5d(17%), and Ir 6p (10%).

From the above results, one can state that the p electrons of Si(1,2) atoms and the d electrons of Ir and La atoms make significant influences on the superconducting properties of $LaIrSi_3$ in accordance with the McMillan-Hopfield expression, which is given as

$$\lambda = \frac{N(E_F)\langle I^2\rangle}{M\langle\omega^2\rangle}, \tag{1}$$

where $\langle\omega^2\rangle$ is the average of squared phonon frequencies, M is the average atomic mass, and $\langle I^2\rangle$ shows the Fermi surface average of squared electron-phonon coupling interaction. This expression shows that a larger value of $N(E_F)$ increases the value of electron-phonon coupling parameter (λ). As we mentioned before, the total contribution of Si(1,2) electronic states is around 43%. Thus, we can conclude that the main effect on the superconducting properties of this material arises from the p states of these atoms. A similar observation has been made for the remaining NCS. In particular, the value of $N(E_F)$ for $LaRhSi_3$ amounts to be 1.78 states/eV with SOI, which is almost equal to the value of 1.76 states/eV without SOI. The values of $N(E_F)$ for $LaPdSi_3$ are found to be 1.49 states/eV and 1.50 states/eV with and without SOI, respectively. As a consequence, we can state that the influence of SOI on the energy bands close to the Fermi level is negligible for both materials. This result is not surprising because the masses of Rh and Pd atoms are much lighter than the mass of Ir atom.

IV. PHONONIC AND ELECTRON-PHONON INTERACTION PROPERTIES

The group theoretical treatment of zone-centre phonon modes in the body-centred tetragonal $BaNiSn_3$ structure (which $LaIrSi_3$, $LaRhSi_3$, and $LaPdSi_3$ assume) with space group I4/mm produces the following irreducible representation:

$$\Gamma = 4E + B_1 + 3A_1, \tag{2}$$

where B_1 and A_1 are the single modes, while E is the modes that doubly degenerate. All phonon modes are both Raman and Infrared active except the B_1 mode which is only Raman active. We have a comparison of the zone-center phonon frequencies with their electron-phonon coupling parameters and their polarization characters for all the studied NCS in

TABLE II. Calculated zone-centre phonon frequencies (ν in THz) with their electron-phonon coupling parameters (λ) and their irreducible representations (polarisation characters—PC) for $LaTSi_3$(T = Ir, Rh, and Pd).

$LaIrSi_3$								
Mode	E	A_1	E	E	B_1	A_1	E	A_1
ν	3.351	3.878	4.634	8.051	8.459	8.946	11.032	11.061
λ	0.086	0.106	0.064	0.081	0.141	0.043	0.021	0.123
PC	La+Ir+Si2+Si1	La+Ir+Si1	Si2+Si1	Si2+Si1	Si2	Si2+Si1+Ir	Si2+Ir	Si2+Si1
$LaRhSi_3$								
Mode	E	A_1	E	E	B_1	A_1	A_1	E
ν	3.790	4.099	4.358	7.980	8.279	8.932	10.470	10.471
λ	0.082	0.141	0.077	0.073	0.158	0.050	0.186	0.027
PC	La+Rh+Si2+Si1	La+Rh+Si1+Si2	Si2+Si1+Rh	Si1+Si2	Si2	Si2+Si1+Rh	Si2+Si1	Si2+Si1
$LaPdSi_3$								
Mode	E	A_1	E	A_1	B_1	E	E	A_1
ν	3.140	3.490	4.050	7.760	8.381	8.418	9.295	10.685
λ	0.106	0.204	0.120	0.087	0.233	0.077	0.080	0.321
PC	La+Pd+Si2+Si1	La+Pd+Si1+Si2	Si2+Si1+Pd	Si2+Si1+Pd	Si2	Si1+Si2	Si2+Si1+Pd	Si2+Si1

Table II. The first point to note that is the doubly degenerate E modes originate from the vibrations of related atoms in the *x*–*y* plane, while the vibrations of relevant atoms along the *z* axis represent the A_1 and B_1 phonon modes. As can be seen from this table, the B_1 phonon modes of all the studied NCS have the largest electron-phonon coupling parameter. A similar observation has been made for $CaIrSi_3$ (Ref. 35) in our previous theoretical study. Further examination of Table II reveals that the electron-phonon coupling parameter for the lowest and the highest A_1 phonon modes is larger than the corresponding parameter for the remaining of zone-centre phonon modes. Thus, eigen representations of these phonon modes are displayed in Fig. 3. The B_1 phonon mode is totally dominated by the motion of Si2 atoms along the **z** direction. This finding totally coincides with our results for $N(E_F)$, which contains the largest contribution from the p states of Si2 atom. It is worth to mention that the A_1 phonon modes also include atomic vibrations of related atoms along the **z** direction.

A trustworthy calculation of electron-phonon coupling requires the knowledge of the full phonon spectrum as well as the corresponding phonon density of states. The calculated phonon dispersion curves along several high symmetry directions of the body-centred tetragonal Brillouin zone for $LaIrSi_3$ are displayed in Fig. 4(a). There are three forbidden gaps with the frequency values of 1.1, 0.2, and 0.9 in the corresponding phonon spectrum. These gaps divide this phonon spectrum into four separate regions. Three acoustic and five

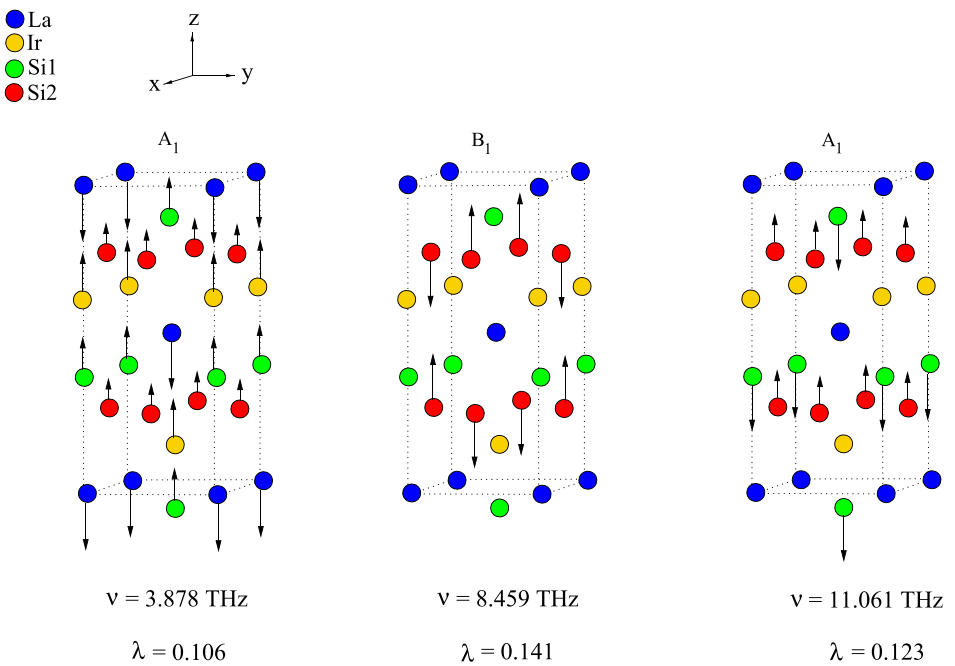

FIG. 3. Eigen atomic displacement patterns for the zone-centre lowest A_1, B_1, and the highest A_1 modes in $LaIrSi_3$. The corresponding phonon modes in the remaining NCS have similar eigen atomic displacement patterns to their counterpatterns in $LaIrSi_3$.

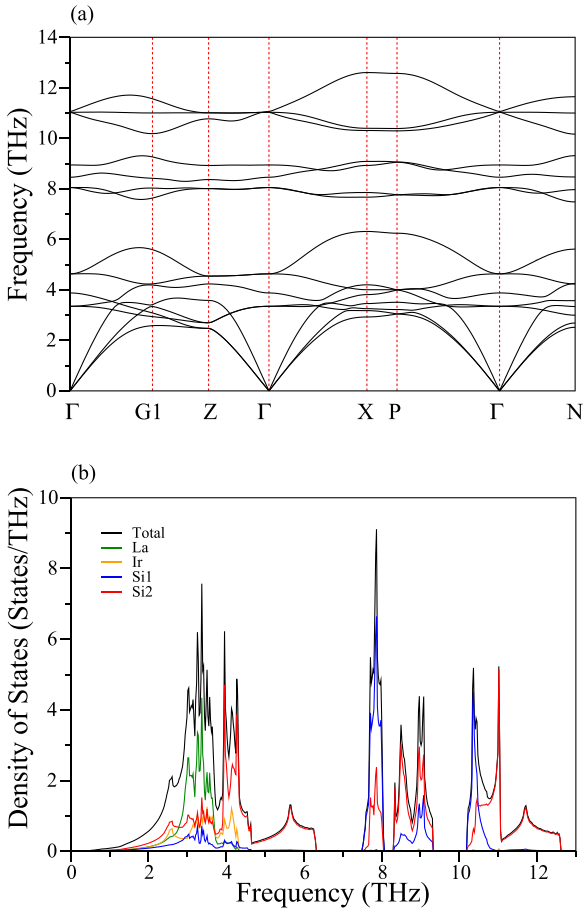

FIG. 4. (a) The phonon dispersion curves for $LaIrSi_3$ along selected symmetry directions in the body-centred tetragonal Brillouin zone. (b) The total and partial phonon density of states for $LaIrSi_3$.

optical phonon modes constitute the first frequency region. The acoustic phonon branches disperse up to around 4 THz in this frequency region, while the five optical branches lie between 3 and 6.4 THz in this region. There is a considerable degree of overlap between low-frequency optical phonon branches and the acoustic phonon branches. Both the second and third frequency regions include two optical phonon branches which are less dispersive than the corresponding optical phonon branches in the first frequency region. These two regions are separated from each other by a narrow gap of 0.2 THz. The fourth last frequency region contains three dispersion optical phonon modes extending the spectral range from 10.2 to 12.7 THz.

The contributions of atomic vibrations to phonon branches can be much better understood by the total and partial phonon DOS. The total phonon DOS and partial DOS are illustrated in Fig. 4(b). The Si1 and Si2-related phonon states are quite dispersive, spreading in lattice vibrations over the whole range of phonon frequencies due to their lighter mass as compared to the masses of remaining atoms, while La and Ir vibrations almost disappear above 4.7 THz because of their heavier masses. In particular, motion implying all three atomic species types are present below 4.7 THz, while the partial DOS exhibits a dominance of La atoms in the frequency region between 2.8 and 3.7 THz. On the other hand, the Si2 atoms dominate the vibrations between 3.7 and 4.7 THz with a minor contribution from the rest of atoms. The frequency region from 4.7 to 6.4 THz is totally contributed by the vibrations of Si2 atoms, while the Si1 atoms seem motionless in this frequency region. The DOS features between 7.5 and 8.1 THz are formed by the vibrations of Si1 atoms with considerable amount of Si2 vibrations. We have to note that the opposite picture can be seen in the frequency region from 8.3 to 9.4 THz. Three peaks with frequencies of 10.4, 11.0, and 11.7 THz are found in the fourth frequency region. The lowest of these vibrational modes is characterized by the motion of Si1 atoms while the rest of them arise from the vibrations of Si2 atoms.

The results for the phonon dispersion relations of $LaRhSi_3$ are displayed in Fig. 5(a) along selected symmetry directions of the body-centred tetragonal Brillouin zone together with the corresponding total and partial DOS in Fig. 5(b). The phonon spectrum of $LaRhSi_3$ looks similar to that of $LaIrSi_3$. First, the absence of imaginary frequency in all high symmetry directions for $LaRhSi_3$ also states the dynamical stability of this material in the body-centred tetragonal $BaNiSn_3$ structure. Second, the phonon spectrum of $LaRhSi_3$ is also divided into four separate regions by three phonon band gaps of 1.2, 0.2, and 0.3 THz. Third, these regions in $LaRhSi_3$ contain the same number of phonon branches as their counter-patterns in $LaIrSi_3$. However, different from

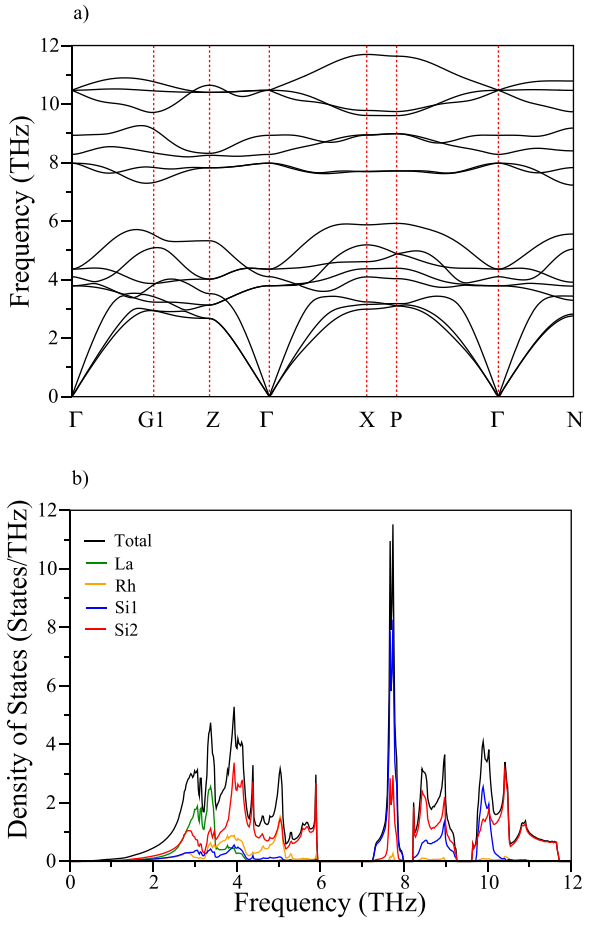

FIG. 5. (a) The phonon dispersion curves for $LaRhSi_3$ along selected symmetry directions in the body-centred tetragonal Brillouin zone. (b) The total and partial phonon density of states for $LaRhSi_3$.

$LaIrSi_3$, three acoustic phonon branches are separated from the low-frequency optical phonon branches along the Γ-X, X-P, and P-Γ directions. The phonon DOS in Fig. 5(b) is split into the contributions of the vibrational phonon modes related to La, Rh, Si1, and Si2. All atomic species contribute to the DOS features below 4.3 THz, while the partial DOS of La atoms are almost negligible above this frequency region due to the heaviest mass of La. In the frequency window from 4.3 to 5.0 THz, a strong hybridization between Si2 and Rh atoms is observed due to a strong covalent bond between these atoms. The largest contribution to DOS from 5.0 to 5.9 THz originates from Si2 vibrational modes with much smaller contribution from Rh vibrational modes. Above the first gap region, the DOS features are pictured by the coupled motion of Si1 and Si2 atoms. However, different from $LaIrSi_3$, the contribution of Rh atoms to these DOS features is appreciable. Due to this reason, the phonon DOS of $LaRhSi_3$ extends up to 11.70 THz, which is 1.0 THz smaller than that of $LaIrSi_3$.

Figure 6(a) presents the calculated phonon spectra for $LaPdSi_3$, while the total and partial DOS for these materials are illustrated in Fig. 6(b). Once again, the calculated phonon spectra have only positive frequencies, at any chosen $\boldsymbol{q}$ wave vector, indicating the dynamical stability of $LaPdSi_3$. Different from the other two NCS, the phonon modes in this material split into only two regions: low-frequency region (LFR) (0–6.3 THz) and high frequency region (HFR) (6.7–10.7 THz), which are separated from each other by a narrow gap of 0.4 THz. The LFR is composed of three acoustic and five optical branches, while seven optical phonon modes appear in the HFR. The three acoustics phonon modes as well as the 12 optical phonon modes in $LaPdSi_3$ are all very dispersive. In agreement with $LaRhSi_3$, three acoustic phonon branches do not overlap with the low-frequency optical phonon branches along the Γ-X, X-P, and P-Γ directions. The calculated total and partial DOS for $LaPdSi_3$, as shown in Fig. 6(b), span the frequency range from 0 to 10.7 THz, which is 1.0 THz smaller than that of $LaRhSi_3$. This decrease in the range of phonon DOS for $LaPdSi_3$ can be linked to the slightly larger volume or heavier mass of Pd of $LaPdSi_3$ as compared with that of $LaRhSi_3$ (see also Table I). The partial DOS for each atom is in accordance with their atomic mass. The LFR is composed of the acoustic and optical phonon vibrations of all non-equivalent atoms. In particular, La, as the heaviest element, dominates the lower frequencies below 3.0 THz with some contribution from the remaining atoms. The DOS features in the HFR originate from the coupled motion of different types of Si atoms, which is quite expected since Si is much lighter than La and Pd. Although La does not make any contribution to the HFR, a much smaller Pd contribution to this region is observed.

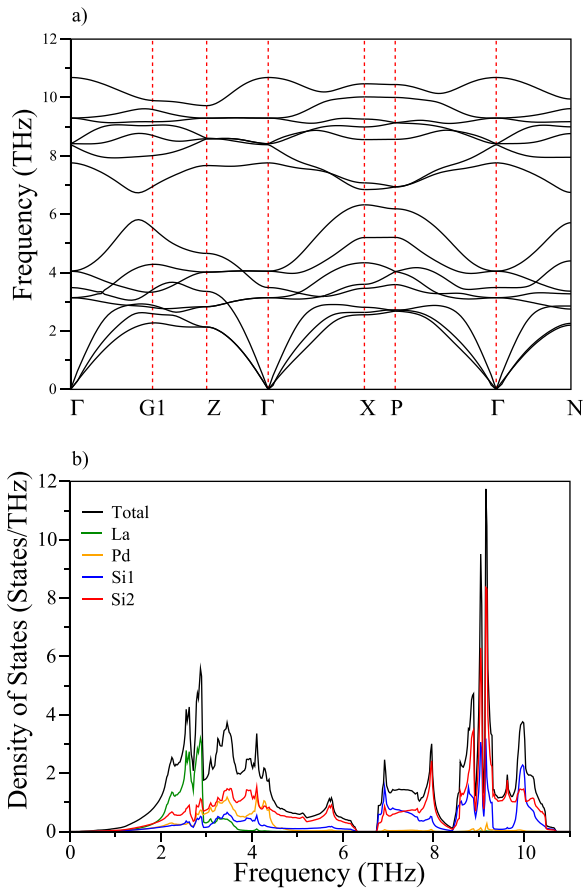

FIG. 6. (a) The phonon dispersion curves for $LaPdSi_3$ along selected symmetry directions in the body-centred tetragonal Brillouin zone. (b) The total and partial phonon density of states for $LaPdSi_3$.

In order to analyze the signature of atoms and their vibrational modes which contribute to superconductivity in $LaIrSi_3$, $LaRhSi_3$, and $LaPdSi_3$ by coupling to the electrons at the Fermi energy, we illustrate their Eliashberg function $\alpha^2F(\omega)$ and frequency accumulated electron-phonon coupling parameter $\lambda(\omega)$ with and without SOI in Fig. 7. This figure clearly shows that the effect of SOI on the electron-phonon interaction in $LaIrSi_3$ is more than that in the remaining NCS which can be linked to the heavier mass of Ir than the masses of Rh and Pd atoms. With the calculated $\alpha^2F(\omega)$,[38,43] one is able to determine the average electron-phonon coupling parameter λ. The calculated values of λ are found to be 0.39, 0.48, and 0.49 for $LaIrSi_3$, $LaPdSi_3$, and $LaRhSi_3$, respectively, which suggests that the electron-phonon interaction in $LaPdSi_3$ and $LaRhSi_3$ is slightly stronger than that in $LaIrSi_3$. Thus, we can conclude that $LaIrSi_3$ displays superconductivity with a lower superconducting critical temperature (T_c) than the other two NCS. The calculated contributions to λ from the LFR (below the first gap region) and the HFR (above the first gap region) are found to be around 60% and 40%, respectively, for all the studied NCS. Although the largest contribution to λ comes from three acoustic phonon branches and five low-frequency optical phonon modes, phonon branches in the HFR make also significant contribution to λ. We believe that considerable contribution to λ coming from HFR arises from the light mass of Si and largest contribution of Si(1,2) p electrons to $N(E_F)$ [see Eq. (1)].

For BCS type superconductors, the modified Allen-Dynes formula[38,43] takes the form

$$T_c = \frac{\omega_{\ln}}{1.2}\exp\left(-\frac{1.04(1+\lambda)}{\lambda-\mu^*(1+0.62\lambda)}\right), \qquad (3)$$

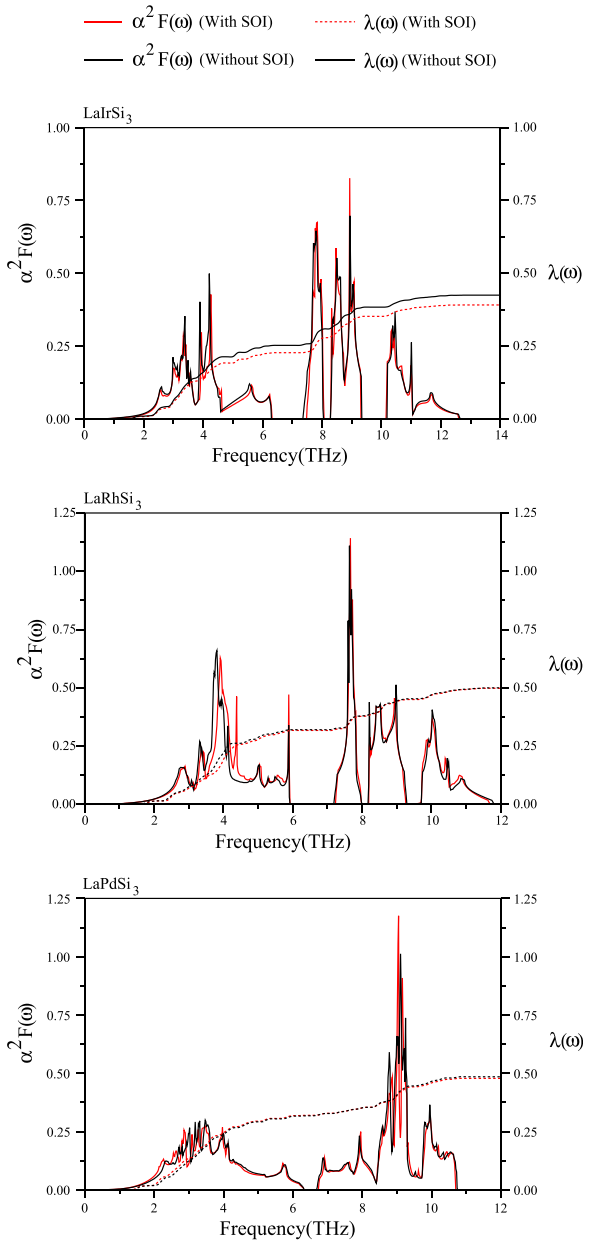

FIG. 7. The calculated Eliashberg spectral function [$\alpha^2F(\omega)$] and electron-phonon coupling parameter (λ) with and without SOI.

which links the value of T_c with λ and the logarithmically averaged phonon frequency ($\omega_{ln} = \exp\left(2\lambda^{-1}\int_0^\infty \frac{d\omega}{\omega}\alpha^2F(\omega)\, ln\omega\right)$), and effective screened Coulomb repulsion ($\mu^* = 0.1$). Furthermore, the electronic specific heat coefficient γ takes the form

$$\gamma = \frac{1}{3}\pi^2 k_B^2 N(E_F)(1+\lambda), \tag{4}$$

which connects the value of γ with $N(E_F)$ and λ. The calculated values of $N(E_F)$, ω_{ln}, λ, T_c, and γ with and without SOI for all the studied NCS are presented in Table III, together with the previous experimental results. In general, the effect of SOI on these superconducting parameters is quite small. In particular, the largest decrease has been observed for the $N(E_F)$ value of $LaIrSi_3$ within 7%. The calculated values of $N(E_F)$, λ, T_c, and γ for all the studied NCS compare very well with their experimental values. Now we can make a comparison of the superconducting parameters $N(E_F)$, ω_{ln}, λ, and T_c between all the studied NCS. As can be seen from Eqs. (1) and (3), the value of T_c will be affected by three parameters such as $N(E_F)$, ω_{ln}, and λ. The largest electron-phonon coupling parameter has been observed for $LaRhSi_3$ due to its largest $N(E_F)$ value. Thus, the calculated T_c for this material is larger than those of the other two NCS studied here.

V. ELASTIC PROPERTIES

In the BCS theory of superconductivity, the electron-phonon interaction is essential for the generation of superconducting states. Since the longwave-length phonon spectrum is mainly related to the elastic properties of the material, these properties of superconducting materials must be studied and discussed. In this work, the second-order elastic constants are calculated using the energies of strained and unstrained geometries.[44] There are six independent elastic constants for tetragonal materials such as C_{11}, C_{12}, C_{13}, C_{33}, C_{44}, and C_{66}. The calculated values are presented in Table IV. These values satisfy the well-known Born's stability criteria (see Ref. 45), confirming that all the considered NCS are mechanically stable in the body-centred tetragonal $BaNiSn_3$ structure. For tetragonal crystals, two Cauchy relations are given as $C_{12} = C_{66}$ and $C_{33} = C_{44}$.[45] The Cauchy

TABLE III. Calculated electron density of states at the Fermi level $N(E_F)$, average electron-phonon coupling parameter λ, superconducting critical temperature T_c, logarithmic frequency ω_{ln}, and electronic specific heat γ values and their comparison with their available previous experimental values for $LaTSi_3$(T = Ir, Rh, and Pd) compounds.

	N (E_F) (states/eV)	λ	ω_{ln} (K)	$\gamma\left(\frac{mJ}{mol\,K^2}\right)$	T_c (K)
$LaIrSi_3$ (with SOI)	1.47	0.39	253.2	4.85	0.89
$LaIrSi_3$ (without SOI)	1.58	0.42	255.2	5.28	1.24
Experimental[30]				4.50	0.77
$LaPdSi_3$ (with SOI)	1.49	0.48	216.5	5.22	2.40
$LaPdSi_3$ (without SOI)	1.50	0.50	220.2	5.21	2.36
Experimental[26]		0.51		4.67	2.65
$LaRhSi_3$ (with SOI)	1.78	0.49	230.2	6.23	2.56
$LaRhSi_3$ (without SOI)	1.76	0.50	236.6	6.20	2.80
Experimental[22]	1.70	0.49		6.04	2.16

TABLE IV. Calculated elastic constants (in GPa) for $LaTSi_3$ materials are shown below. The Debye temperature (Θ_D) and superconductivity transition temperature (T_c) are given in K.

	C_{11}	C_{12}	C_{33}	C_{13}	C_{44}	C_{66}	Θ_D	T_c
$LaIrSi_3$	211.95	67.98	217.21	108.56	41.41	62.57	300	0.90
Experimental[30]							225	0.77
$LaRhSi_3$	185.48	75.96	193.42	97.21	44.87	57.18	367	3.09
Experimental[22]							357	2.16
$LaPdSi_3$	163.88	73.36	162.64	81.28	66.60	48.26	372	3.17
Experimental[26]							397	2.65

relations are totally satisfied if the atoms interact only with the central forces. The calculated results suggest that C_{12}, C_{66}, C_{33}, and C_{44} do not satisfy the Cauchy relations for any of the three NCS studied here. This confirms that non-central forces are crucial for the stability of the crystal structure of all the considered NCS, which exhibit strong covalent interaction between a transition metal and Si atoms. The Debye temperature (Θ_D) is a fundamental attribute of a crystal because it connects elastic properties with thermodynamics properties such as specific heat, melting temperature, and vibrational entropy. A simplified method[46–50] for calculating the Debye temperature from elastic constants has been used. The calculated values of Θ_D for all the studied NCS are also presented in Table IV. These values are comparable with their corresponding experimental values in this table. Finally, inserting the calculated values of Θ_D and λ into the McMillan's formula,[51] the values of T_c are determined to be 0.90, 3.09, and 3.17 K for $LaIrSi_3$, $LaRhSi_3$, and $LaPdSi_3$, respectively, which are in reasonable agreement with their experimental values of 0.77, 2.16, and 2.65 K.[22,26,30] The calculated T_c values are also comparable with the obtained values from the modified Allen-Dynes formula [see Eq. (3)], which are shown in Table III.

VI. SUMMARY

We have reported the structural, elastic, electronic, phononic, and electron-phonon interaction properties of the La-based NCS, such as $LaIrSi_3$, $LaRhSi_3$, and $LaPdSi_3$, adopting the body-centred tetragonal $BaNiSn_3$ type structure, by using the generalized gradient approximation of the density functional theory and the plane wave *ab initio* pseudopotential method. The electronic band structures of all the studied NCS look similar to each other, but the splitting effects due to non-inversion symmetry on $LaRhSi_3$ and $LaPdSi_3$ are less pronounced because of the smaller masses of their transition metals in comparison to the transition metal mass of $LaIrSi_3$. In particular, when the SOI is taken into account, the largest vertical splitting value for $LaIrSi_3$ is found to be 0.35 eV. The observation of small splitting of bands around the Fermi surface may be a sign that a mixing of spin-singlet and spin-triplet components in these NCS is weak and spin-singlet Cooper pairs dominate. The critical assessment analysis of structural and electronic properties of these materials suggests that the bonding in these NCS can be classified as an interplay between covalent, metallic, and ionic characters. Although the largest contribution to $N(E_F)$ comes from the p electrons of Si(1,2), the d electrons of La and transition metal atoms also make considerable contributions to the value of this quantity. This observation indicates the active role of all constituents in determining the electronic and superconducting properties of these NCS.

The calculated Eliashberg spectral function with and without SOI shows that the largest contribution to electron-phonon coupling comes from low frequency phonon modes, but high frequency phonon modes are also involved in the process of scattering of electrons due to the significant existence of Si(1,2) p electrons at the Fermi level. With the inclusion of SOI, the average electron-phonon coupling parameter does not change more than 7%. This small change can be related to the small splitting of electronic bands at E_F. Inserting the values of average electron-phonon coupling parameter and logarithmically averaged phonon frequency into the McMillan formula, the values of superconducting temperatures are found to be 0.89 K for $LaIrSi_3$, 2.40 K for $LaPdSi_3$, and 2.56 K for $LaRhSi_3$. These values compare very well with their experimental values of 0.77, 2.65, and 2.16 K.

Furthermore, using the second-order elastic constants, the Debye temperatures of these NCS are calculated to be 300 K for $LaIrSi_3$, 372 K for $LaPdSi_3$, and 367 K for $LaRhSi_3$. Inserting the values of average electron-phonon coupling parameter and Debye temperature into the McMillan formula, the values of superconducting temperatures are obtained to be 0.90 for $LaIrSi_3$, 3.17 for $LaPdSi_3$, and 3.09 K for $LaRhSi_3$, which are also comparable with their experimental values. Thus, we can conclude that the superconductivity in $LaIrSi_3$, $LaRhSi_3$, and $LaPdSi_3$ must arise from the phonon-mediated electron-phonon interaction with BCS type character.

ACKNOWLEDGMENTS

This work was supported by the Scientific and Technical Research Council of Turkey (TÜBİTAK) (Project No. MFAG-115F135). Some of the calculations for this project were carried out using the Intel Nehalem (i7) cluster (ceres) computing facilities in the School of Physics, University of Exeter, United Kingdom.

[1]Y. D. Seropegina, B. I. Shapieva, A. V. Gribanova, and O. I. Bodak, "Isothermal cross-section of the Ce-Ru-Si phase diagram at 600 °C," J. Alloys Compd. **288**, 147 (1999).

[2]T. Kawai, H. Muranaka, M. A. Measson, T. Shimoda, Y. Doi, T. D. Matsuda, Y. Haga, G. Knebel, G. Lapertot, D. Aoki, J. Flouquet, T. Takeuchi, R. Settai, and Y. Ōnuki, "Magnetic and superconducting

properties of CeTX3 (T: transition metal and X: Si and Ge) with non-centrosymmetric crystal structure," J. Phys. Soc. Jpn. **77**, 064716 (2008).
[3]M. Smidman, D. T. Adroja, E. A. Goremychkin, M. R. Lees, D. M. Paul, and G. Balakrishnan, "Evidence for a hybridization gap in noncentrosymmetric $CeRuSi_3$," Phys. Rev. B **91**, 064419 (2015).
[4]N. Kumar, S. K. Dhar, A. Thamizhavel, P. Bonville, and P. Manfrinetti, "Magnetic properties of $EuPtSi_3$ single crystals," Phys. Rev. B **81**, 144414 (2010).
[5]N. Kumar, P. K. Das, R. Kulkarni, A. Thamizhavel, S. K. Dhar, and P. Bonville, "Antiferromagnetic ordering in $EuPtGe_3$," J. Phys.: Condens. Matter **24**, 036005 (2012).
[6]D. Kaczorowski, B. Belan, and R. Gladyshevskii, "Magnetic and electrical properties of $EuPdGe_3$," Solid State Commun. **152**, 839 (2012).
[7]R. J. Goetsch, V. K. Anand, and D. C. Johnston, "Antiferromagnetism in $EuNiGe_3$," Phys. Rev. B **87**, 064406 (2013).
[8]O. Bednarchuk, A. Gagor, and D. Kaczorowski, "Synthesis, crystal structure and physical properties of $EuTGe_3$ (T = Co, Ni, Rh, Pd, Ir, Pt) single crystals," J. Alloys Compd. **622**, 432 (2015).
[9]A. Maurya, P. Bonville, R. Kulkarni, A. Thamizhavel, and S. K. Dhar, "Magnetic properties and complex magnetic phase diagram in non-centrosymmetric $EuRhGe_3$ and $EuIrGe_3$ single crystals," J. Magn. Magn. Mater. **401**, 823 (2016).
[10]N. Kimura, K. Ito, K. Saitoh, Y. Umeda, H. Aoki, and T. Terashima, "Pressure-induced superconductivity in noncentrosymmetric heavy-fermion $CeRhSi_3$," Phys. Rev. Lett. **95**, 247004 (2005).
[11]N. Egetenmeyer, J. L. Gavilano, A. Maisuradze, S. Gerber, D. E. MacLaughlin, G. Seyfarth, D. Andreica, A. Desilets-Benoit, A. D. Bianchi, C. Baines, R. Khasanov, Z. Fisk, and M. Kenzelmann, "Direct observation of the quantum critical point in heavy fermion $CeRhSi_3$," Phys. Rev. Lett. **108**, 177204 (2012).
[12]H. Mukuda, T. Fujii, T. Ohara, A. Harada, M. Yashima, Y. Kitaoka, Y. Okuda, R. Settai, and Y. Onuki, "Enhancement of superconducting transition temperature due to the strong antiferromagnetic spin fluctuations in the noncentrosymmetric heavy-fermion superconductor $CeIrSi_3$: A ^{29}Si NMR study under pressure," Phys. Rev. Lett. **100**, 107003 (2008).
[13]Y. Tada, N. Kawakami, and S. Fujimoto, "Spin fluctuations and superconductivity in noncentrosymmetric heavy fermion systems $CeRhSi_3$ and $CeIrSi_3$," Phys. Rev. B **81**, 104506 (2010).
[14]M. Szlawska and D. Kaczorowski, "Antiferromagnetic order and Kondo effect in single-crystalline Ce_2IrSi_3," Phys. Rev. B **84**, 094430 (2011).
[15]R. Settai, I. Sugitani, Y. Okuda, A. Thamizhavel, M. Nakashima, Y. Ōnuki, and H. Harima, "Pressure-induced superconductivity in $CeCoGe_3$ without inversion symmetry," J. Magn. Magn. Mater. **310**, 844 (2007).
[16]M. Smidman, D. T. Adroja, A. D. Hillier, L. C. Chapon, J. W. Taylor, V. K. Anand, R. P. Singh, M. R. Lees, E. A. Goremychkin, M. M. Koza, V. V. Krishnamurthy, D. M. Paul, and G. Balakrishnan, "Neutron scattering and muon spin relaxation measurements of the noncentrosymmetric antiferromagnet $CeCoGe_3$," Phys. Rev. B **88**, 134416 (2013).
[17]F. Honda, I. Bonalde, K. Shimizu, S. Yoshiuchi, Y. Hirose, T. Nakamura, R. Settai, and Y. Ōnuki, "Pressure-induced superconductivity and large upper critical field in the noncentrosymmetric antiferromagnet $CeIrGe_3$," Phys. Rev. B **81**, 140507(R) (2010).
[18]H. Q. Yuan, D. F. Agterberg, N. Hayashi, P. Badica, D. Vandervelde, K. Togano, M. Sigrist, and M. B. Salamon, "S -Wave spin-triplet order in superconductors without inversion symmetry:Li_2Pd_3B and Li_2Pt_3B," Phys. Rev. Lett. **97**, 017006 (2006).
[19]T. Takimoto and P. Thalmeier, "Triplet cooper pair formation by anomalous spin fluctuations in non-centrosymmetric superconductors," J. Phys. Soc. Jpn. **78**, 103703 (2009).
[20]E. Bauer, R. T. Khan, H. Michor, E. Royanian, A. Grytsiv, N. Melnychenko-Koblyuk, P. Rogl, R. Reith, R. Podloucky, E.-W. Scheidt, W. Wolf, and M. Marsman, "$BaPtSi_3$: A noncentrosymmetric BCS-like superconductor," Phys. Rev. B **80**, 064504 (2009).
[21]R. Ribeiro-Palau, R. Caraballo, P. Rogl, E. Bauer, and I. Bonalde, "Strong-coupling BCS superconductivity in noncentrosymmetric $BaPtSi_3$: A low-temperature study," J. Phys.: Condens. Matter **26**, 235701 (2014).
[22]V. K. Anand, A. D. Hillier, D. T. Adroja, A. M. Strydom, H. Michor, K. A. McEwen, and B. D. Rainford, "Specific heat and μSR study on the non-centrosymmetric superconductor $LaRhSi_3$," Phys. Rev. B **83**, 064522 (2011).
[23]N. Kimura, N. Kabeya, K. Saitoh, K. Satoh, H. Ogi, K. Ohsaki, and H. Aoki, "Type II/1 superconductivity with extremely high Hc3 in noncentrosymmetric $LaRhSi_3$," J. Phys. Soc. Jpn. **85**, 024715 (2016).
[24]G. Eguchi, D. C. Peets, M. Kriener, Y. Maeno, E. Nishibori, Y. Kumazawa, K. Banno, S. Maki, and H. Sawa, "Crystallographic and superconducting properties of the fully gapped noncentrosymmetric 5 d -electron superconductors $CaMSi_3$(M = Ir, Pt)," Phys. Rev. B **83**, 024512 (2011).
[25]R. P. Singh, A. D. Hillier, D. Chowdhury, J. A. T. Barker, D. McK. Paul, M. R. Lees, and G. Balakrishnan, "Probing the superconducting ground state of the noncentrosymmetric superconductors $CaTSi_3$(T = Ir, Pt) using muon-spin relaxation and rotation," Phys. Rev. B **90**, 104504 (2014).
[26]M. Smidman, A. D. Hillier, D. T. Adroja, M. R. Lees, V. K. Anand, R. P. Singh, R. I. Smith, D. M. Paul, and G. Balakrishnan, "Investigations of the superconducting states of noncentrosymmetric $LaPdSi_3$ and $LaPtSi_3$," Phys. Rev. B **89**, 094509 (2014).
[27]V. K. Anand, D. Britz, A. Bhattacharyya, D. T. Adroja, A. D. Hillier, A. M. Strydom, W. Kockelmann, B. D. Rainford, and K. A. McEwen, "Physical properties of noncentrosymmetric superconductor $LaIrSi_3$: A μSR study," Phys. Rev. B **90**, 014513 (2014).
[28]M. Isobe, M. Arai, and N. Shirakawa, "Superconductivity in noncentrosymmetric $SrAuSi_3$," Phys. Rev. B **93**, 054519 (2016).
[29]T. Terashima, M. Kimata, S. Uji, T. Sugawara, N. Kimura, H. Aoki, and H. Harima, "Fermi surface in $LaRhSi_3$ and $CeRhSi_3$," Phys. Rev. B **78**, 205107 (2008).
[30]Y. Okuda, Y. Miyauchi, Y. Ida, Y. Takeda, C. Tonohiro, Y. Oduchi, T. Yamada, N. D. Dung, T. D. Matsuda, Y. Haga, T. Takeuchi, M. Hagiwara, K. Kindo, H. Harima, K. Sugiyama, R. Settai, and Y. Ōnuki, "Magnetic and superconducting properties of $LaIrSi_3$ and $CeIrSi_3$ with the non-centrosymmetric crystal structure," J. Phys. Soc. Jpn. **76**, 044708 (2007).
[31]V. V. Bannikov, I. R. Shein, and A. L. Ivanovskii, "Structural and electronic properties and the fermi surface of the new noncentrosymmetric superconductors: 3.6 K $CaIrSi_3$ and 2.3 K $CaPtSi_3$," JETP Lett. **92**, 343 (2010).
[32]J. Kaczkowski and A. Jezierski, "First-principle study on electronic and structural properties of newly discovered superconductors: $CaIrSi_3$ and $CaPtSi_3$," J. Alloys Compd. **509**, 6142 (2011).
[33]M. J. Winiarski and M. Samsel-Czekala, "Electronic structure of non-centrosymmetric superconductor $LaPdSi_3$ and its reference compound $LaPdGe_3$," Intermetallics **56**, 44 (2015).
[34]E. Arslan, E. Karaca, H. M. Tütüncü, A. Başoğlu, and G. P. Srivastava, "Theoretical investigation of superconductivity in $SrAuSi_3$ and $SrAu_2Si_2$," J. Phys. Chem. Solids **95**, 65 (2016).
[35]H. Y. Uzunok, E. İpsara, H. M. Tütüncü, G. P. Srivastava, and A. Başoğlu, "The effect of spin orbit interaction for superconductivity in the noncentrosymmetric superconductor $CaIrSi_3$," J. Alloys Compd. **681**, 205 (2016).
[36]A. B. Migdal, "Interaction between electrons and lattice vibrations in a normal metal," Zh. Eksp. Teor. Fiz. **34**, 1438 (1958) [ZhETF, **34**, 1438 (1958)].
[37]G. M. Eliashberg, "Interactions between electrons and lattice vibrations in a superconductor," Sov. Phys. JETP **11**, 696 (1960) [ZhETF, **38**, 966 (1960)].
[38]P. B. Allen and R. C. Dynes, "Transition temperature of strong-coupled superconductors reanalyzed," Phys. Rev. B **12**, 905 (1975).
[39]P. Giannozzi, S. Baroni, N. Bonini, M. Calandra, R. Car, C. Cavazzoni, D. Ceresoli, G. L. Chiarotti, M. Cococcioni, I. Dabo, A. D. Corso, S. de Gironcoli, S. Fabris, G. Fratesi, R. Gebauer, U. Gerstmann, C. Gougoussis, A. Kokalj, M. Lazzeri, L. Martin-Samos, N. Marzari, F. Mauri, R. Mazzarello, S. Paolini, A. Pasquarello, L. Paulatto, C. Sbraccia, S. Scandolo, G. Sclauzero, A. P. Seitsonen, A. Smogunov, P. Umari, and R. M. Wentzcovitch, "QUANTUM ESPRESSO: A modular and open-source software project for quantum simulations of materials," J. Phys.: Condens. Matter **21**, 395502 (2009).
[40]J. P. Perdew, K. Burke, and M. Erzerhof, "Generalized gradient approximation made simple," Phys. Rev. Lett. **77**, 3865 (1996).
[41]W. Kohn and L. J. Sham, "Self-consistent equations including exchange and correlation effects," Phys. Rev. **140**, A1133 (1965).
[42]H. J. Monkhorst and J. D. Pack, "Special points for Brillouin-zone integrations," Phys. Rev. **13**, 5188 (1976).
[43]H. M. Tütüncü, H. Y. Uzunok, E. Karaca, G. P. Srivastava, S. Özer, and Ş. Uğur, "Ab initio investigation of BCS-type superconductivity in $LuNi_2B_2C$-type superconductors," Phys. Rev. B **92**, 054510 (2015).
[44]M. J. Mehl, J. E. Osburn, D. A. Papaconstantopoulos, and B. M. Klein, "Structural properties of ordered high-melting-temperature intermetallic

alloys from first-principles total-energy calculations," Phys. Rev. B **41**, 10311 (1990).
[45]M. Born and K. Huang, *Dynamical Theory of Crystal Lattices* (Clarendon, Oxford, 1956).
[46]W. Voigt, *Lehrbuch der Kristallphysik* (Taubner, Leipzig, 1928).
[47]A. Reuss and Z. Angew, "Calculation of the yield point of mixed crystals," Math. Mech. **9**, 55 (1929).
[48]R. Hill, "The elastic behaviour of a crystalline aggregate," Proc. Phys. Soc. London A **65**, 349 (1952).
[49]O. L. Anderson, "A simplified method for calculating the Debye temperature from elastic constants," J. Phys. Chem. Solids **24**, 909 (1963).
[50]P. Ravindran, L. Fast, P. A. Korzhavyi, B. Johansson, J. Wills, and O. Eriksson, "Density functional theory for calculation of elastic properties of orthorhombic crystals: Application to $TiSi_2$," J. Appl. Phys. **84**, 4891 (1998).
[51]W. L. McMillan, "Transition temperature of strong-coupled superconductors," Phys. Rev. **167**, 331 (1968).